

Microstructural evaluation of welded joints of ASTM Mar-M247 superalloy using ERNiCrMo-3 filler alloy

Bassam Salman Alomairi¹ , Zied Driss¹, Adnan Naama Abood²

¹University of Sfax, National School of Engineering of Sfax, Laboratory of Electro-Mechanic Systems. Sfax, Tunisia.

²Middle Technical University, Technical Engineering College. Baghdad, Iraq.

e-mail: bassam.alomairy45@gmail.com, zied.driss@enis.tn, adnan_naama_59@yahoo.com

ABSTRACT

ASTM Mar-M247 is one of the superalloys used to manufacture gas turbine blades in power stations. This paper studies the microstructure across welded joints of a turbine blade made of a high-strength material (Mar-M247 alloy) employing AWS ERNiCrMo-3 as a filler alloy. This process was carried out using gas tungsten arc welding (GTAW). The dendritic and interdendritic structures were observed in the fusion zone. The results also showed the presence of epitaxial growth at the interface between the weld metal and the base alloy without solidification cracks. Al and Co concentrations gradually decrease towards the weld metal zone during the solidification process, while Cr content increases towards the fusion zone. Vickers hardness revealed that the hardness in the heat-affected zone (HAZ) is higher than that of the base metal and the weld metal zone, the average in the HAZ is 340HV, while in the base metal and the fusion zone is 322HV, 284HV respectively. Coarse grains in the HAZ were found with an agglomeration of carbides at the grain boundaries due to the input heat of the welding process.

Keywords: Gas turbine blade; Mar-M247; GTAW; Filler alloy; Microstructure; Hardness.

1. INTRODUCTION

Mar-M247 alloy is one of the superalloys based on nickel in its composition that has a polycrystalline microstructure. This alloy was developed by Danesi and Lund for Martin Corporation in 1970 [1]. The optimum specifications of this alloy in terms of design and control of the microstructure make the Mar-M247 alloy widely used in high-temperature-base applications, such as gas turbine blades and aircraft engines. In addition, it has good resistance to creep and corrosion at high temperatures. The casting technique used in manufacturing this alloy is conventional casting [2]. Besides, its balanced chemical composition makes the alloy more acceptable in terms of microstructure and thermal stability up to a temperature of 1000 °C [3, 4]. As mentioned above, gas turbine blades are one of the applications of Mar-M247 superalloy, which are exposed to high temperatures, especially in the first stage of gas turbine blades. Also, the blades and other components of the hot path of gas turbines experience service-induced degradation during operation, which may be normal or hastened owing to multiple factors such as thermal fatigue, creep, and corrosion. Thus, these blades require regular maintenance to avoid unexpected dangers [5–8]. Today competition to improve power plants has increased the ability to carry out many continuous maintenance processes, which leads to high efficiency and safety standards [9]. Due to the high cost of producing components for hot sections of power plants turbines, and aircraft engines, the fusion welding process can repair the damaged parts and rehabilitate them [10]. The complex chemical composition of this alloy makes it a non-weldable alloy, especially its high content of Al and Ti [11]. Acquiring the epitaxial mode of solidification and strengthening creep resistance in the melting zone is the biggest hurdle in the welding process of this type of alloy for reducing dislocations in the alloy with long-term service [12, 13]. Among existing welding processes, GTAW is typically used for precision, stability, excellent solder appearance, and quality in advanced, fine, or ultra-fine materials. Also, it can be used for cladding critical sections, especially for marine equipment because of its very high-quality welds [14, 15]. GTAW is one of the most common techniques in fusion welding. This technology is commonly employed in many industrial applications due to its low cost and good efficiency [16]. In addition, arc welding by gas tungsten can be performed manually, especially at power plants, compared to electron beam welding (EBW), which requires a vacuum chamber, thereby giving further restrictions to the use of this type of fusion welding [17–19]. There are certain limitations of using

GTAW such as bottom joint penetration, inability to weld thick metals that increase more than 3 mm in a single pass, and weak tolerance to numerous compositions when compared to gas metal arc welding. Filler alloys are used in the welding process and consumed by fusion welding methods such as GTAW to fill the gap between two close-fitting materials. When heated, these alloys melt and flow into the gaps between two materials to form the weld joint. Filler alloys have excellent melting temperature and flow qualities to allow capillary action to distribute them in prepared joints. Welders rarely employ filler metals when welding thinner materials, flanges, or edge joints. Welders, on the other hand, generally employ externally fed filler metal for thicker materials. Also, joints made of filler metals are strong and resistant to corrosion, and they also meet other service criteria [20, 21]. These alloys also largely meet the requirements of the American Welding Society (AWS), the American Society for Testing Materials (ASTM), and ISO standards. The ability to perform field maintenance significantly reduces overall costs and increases production. However, there is a high thermal input accompanied during the welding process, which causes some metallurgical problems like solidification cracks and micro-fissuring in the fusion zone [10, 22]. Many researchers investigated the possibility of using filler alloys for welding joints of superalloys. They have shown that filler alloys based on nickel are the optimal choice in welding [23, 24]. OLLA *et al.* [9] studied the weldability of the steam turbine blade (stainless steel) using Inconel-82 as the filler metal, and also the microstructure and the diffusion of elements across the weldments. They found that the migrating grain boundaries are prevalent in the fusion zone. Also, the diffusion of the Fe element in the weld-metal zone is better than Cr and Ni elements. SHARMA *et al.* [25] investigated the multi-pass welding between Hastelloy C 276 and stainless steel type 321 using GTAW with AWS ERNiCrMo-4 as a filler alloy. They revealed a change in the microstructure from columnar to cellular structure when the parameters of the welding passes changed. KARAHAN *et al.* [26] studied the weldability and microstructure analysis for welding alloys of stainless steel and Inconel 625 by Metal Inert Gas (MIG). The researchers found that precipitations rich in Mo, and Ti elements lie between the dendritic arms. This study aims to verify the microstructure of welded specimens of ASTM Mar-M247 alloy taken from a gas turbine blade by the filler alloy of type AWS ERNiCrMo-3, thus assessing the weldability of this alloy. The novelty of this study lies in the investment of its results in the maintenance and repair of gas turbine blades. Although the published studies in the welding of this type of alloy were limited, this study relies on two primary axes: the microstructural characterization of the received material and the knowledge of its structures and phases; the possibility of welding this type of alloy and studying the microstructure of welded joints and the diffusion of alloying elements along the weld.

2. MATERIALS AND METHODS

2.1. Alloys and welding joint design

ASTM Mar-M247 alloy was used as the base alloy taken from a consumed gas turbine blade, as shown in Figure 1a. In this work, AWS ERNiCrMo-3 was employed as a filler alloy, which has a diameter of 2.4 mm. Table 1 indicates the chemical analysis and the mechanical properties of the substrate and the filler alloy. The used materials are chemically analysed using optical emission spectrometer device. The gas turbine blade was cut from the root zone of the blade using a wire-cutting machine to obtain a pair of symmetrical pieces, as indicated in Figure 1b. The specimens have approximate dimensions of $50 \times 10 \times 5$ mm. The selected geometric joint was a butt weld joint of type a single V-groove with a 1.5 mm root face, 1.7 mm gap size, and an inclined angle of 70° as shown in Figure 1c. The welding process was carried out by the TIG machine of type JASIC Tig 200 S using two passes to achieve the weld. The diameter of the tungsten electrode type 2% thoriated tungsten used in the welding is 2.4 mm. The used parameters of the welding technique are shown in Table 2. Also, the high welding efficiency depends on the welder's skill. Preheating of the samples was not performed before the welding. After welding, the welded joints were transversely sectioned into small pieces using Electrical Discharge Machine (EDM). The sectioned specimens have constant dimensions of $20 \times 10 \times 5$ mm.

2.2. Metallographic examination

To prepare welded samples for microstructure examination, the grinding process was applied to the cross-sections of the welded specimens using different grades of emery papers, ASTM grid 400 to 1200. The polishing process was carried out using a special cloth with small amounts of diamond paste to obtain mirror surfaces without scratches. According to the standard ASTM E407 [27, 28], the etching process was performed to reveal the microstructure using chemical solutions with weight percentages of 80% HCl and 20% HNO_3 .

2.3. Tests characterization

An optical microscope (Nikon, Japan), and scanning electron microscope (SEM) (Vega3, Oxford, England) were used to diagnose and analyze the microstructure. The line mapping analysis was applied to diagnose the

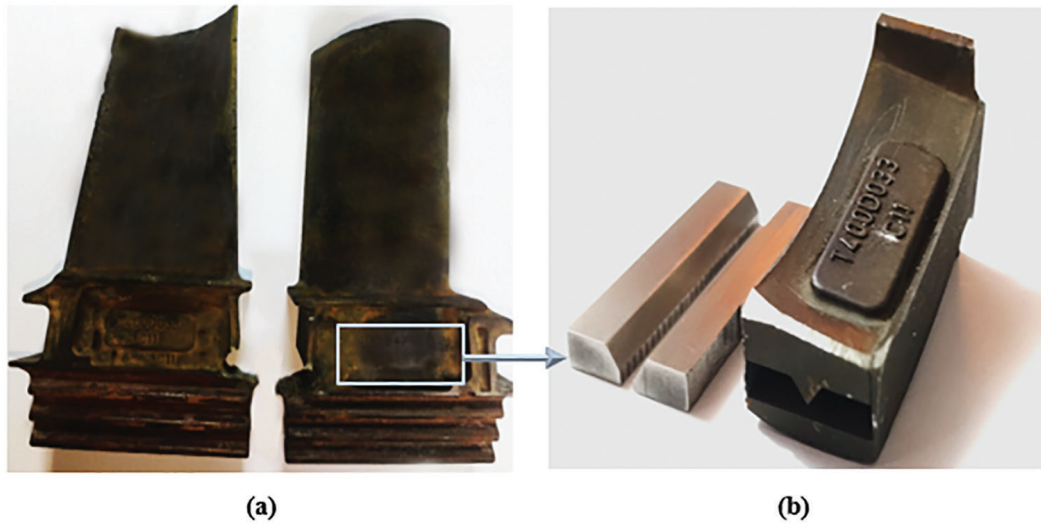


Figure 1: Configuration welding joint of a gas turbine blade: (a) used gas turbine blades (b) cross-section of the root region of the blade (c) diagram showing butt weld joint (V groove).

Table 1: Actual chemical analysis and general mechanical properties of the base alloy and a filler alloy.

MATERIAL	ALLOY ELEMENTS (WEIGHT %)								
	Al	Cr	C	Co	W	Ti	Mn	Mo	Ni
Mar-M247	5.3	8.3	0.11	10	10.3	0.9	0.02	0.94	Bal
ER NiCrMo-3	0.06	19	0.02	–	–	–	1.4	6.19	Bal
USED MATERIALS	NOMINAL MECHANICAL PROPERTIES OF ASTM MAR-M247 AND FILLER ALLOY								
	0.2% YIELD POINT (Mpa)			TENSILE STRENGTH (Mpa)			ELONGATION (%)		
Mar-M247	965			815			4.8		
ERNiCrMo-3	290–414			724–896			65–40		

Table 2: Parameters of welding in this work.

POLARITY TYPE	WELDING CURRENT	WELDING VOLTAGE	WELDING POSITION	A FLOW RATE OF SHIELDED GAS	ARGON PURITY
DCEN	120 A	78 V	Flat	10 L/min	99.999%

diffusion of elements along the welding regions by EDS (Vega3, England) attached to SEM. To identify the crystalline phases in the substrate and the welded specimen, X-ray diffraction (Shimadzu XRD/6000, Tokyo, Japan) with Cu-K radiation was employed, and a current of 30 mA, a voltage of 40 kV, and an angular range of 10°–120°. The Vickers microhardness was performed using a digital device (HVS-1000) with of 30 g load for 15 s through a set of points along the weld joint.

3. RESULTS AND DISCUSSION

3.1. Microstructural examination

3.1.1. Microstructure of the base alloy Mar-M247

The microstructure of the Mar-M247 alloy reveals coarse grains formed during the solidification stage with the presence of MC carbide between the grain boundaries, as detailed in Figure 2a. The morphology of MC carbide is similar to the Chinese script that widely appears in ASTM Mar-M247 alloy, as shown in Figure 2b. In addition,

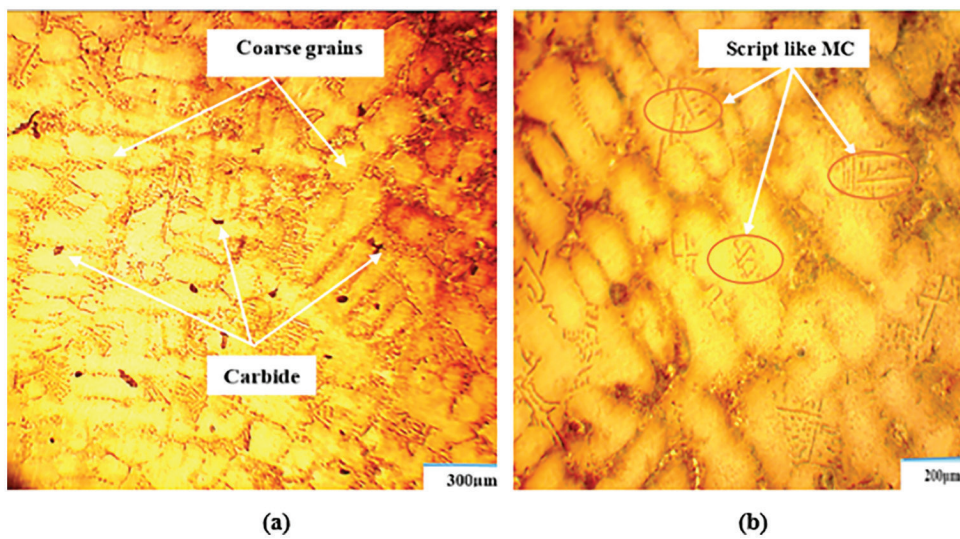


Figure 2: Microstructure images of ASTM Mar-M247 alloy as a base alloy: (a) coarse grain of alloy Mar-M247 (b) morphology of script-like carbide in Mar-M247 superalloy.

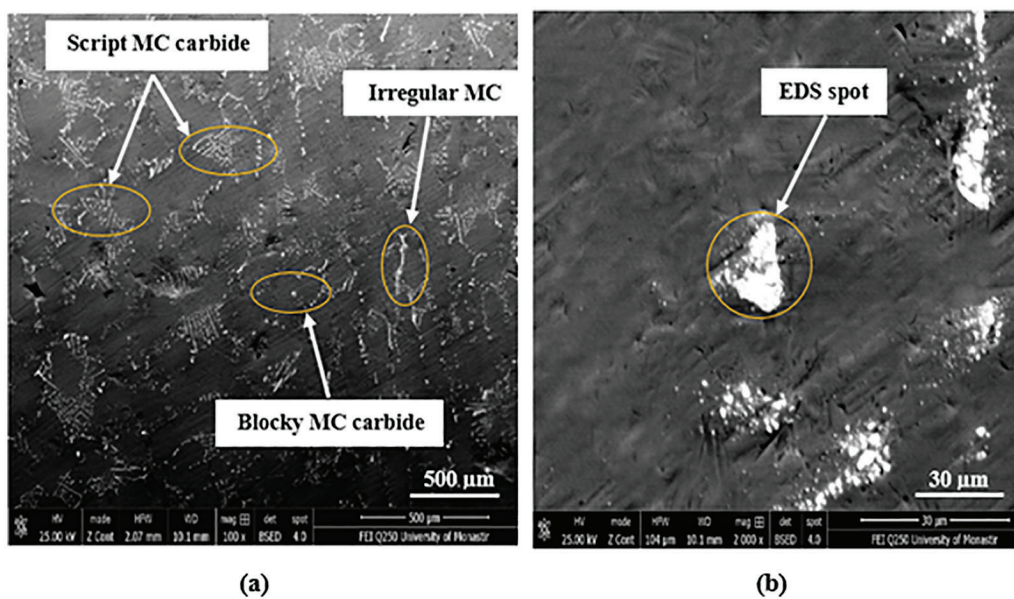


Figure 3: SEM microstructure of ASTM Mar-M247 alloy (a) morphology of MC carbides without etching process (b) high magnification SEM image (2000x) showing MC carbide.

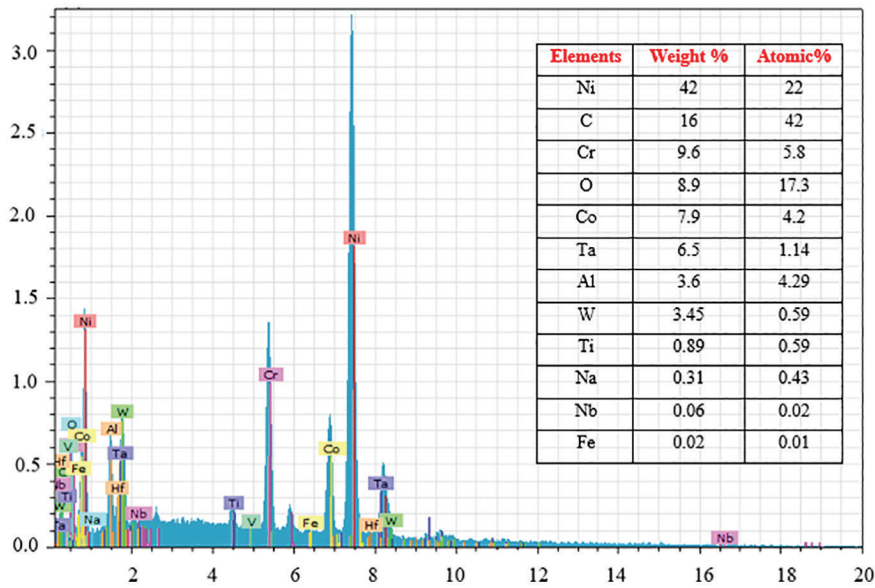


Figure 4: Point analysis by EDS of MC carbides in ASTM Mar-M247alloy.

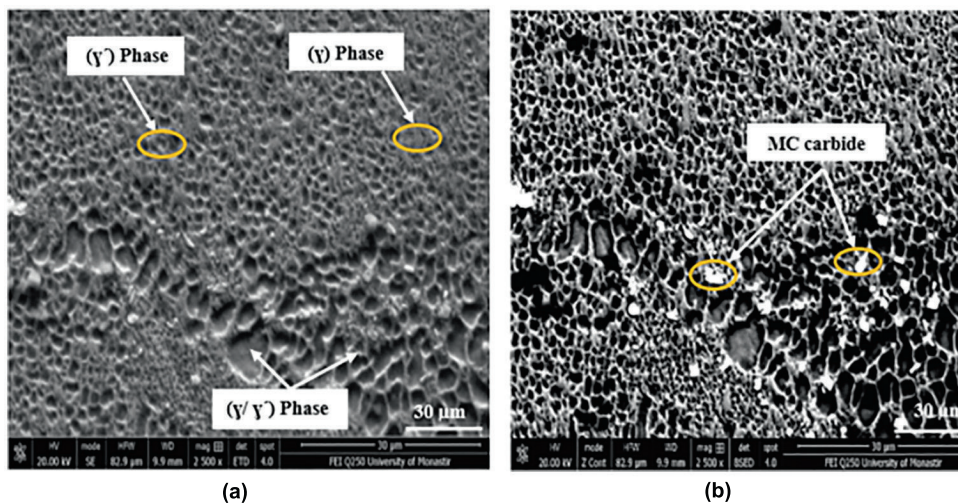


Figure 5: SEM images showing the microstructure of the base alloy Mar-M247: (a) phases of ASTM Mar-M247 alloy (b) MC carbide image using BSED detector.

various shapes of MC carbide can be found in the microstructure of ASTM Mar-M247 alloy, such as blocky, and irregular as shown in Figure 3a. The blocky morphology of MC carbide in Figure 3b was analysed according to the EDS analysis, and it is rich in Ta, Ti, Nb, and C, as shown in Figure 4. These elements tend to segregate and combine with C to form the primary carbides at the intergranular zone and grain boundaries [29, 30]. The phases of gamma γ and gamma prime γ' of ASTM Mar-M247 alloy can be diagnosed using SEM, as illustrated in Figure 5. The matrix phase γ is the alloy's main phase, which strengthens by the precipitated particles of the gamma prime (Ni_3Al), thus reducing dislocation movements and increasing the strength at elevated temperatures [31]. In addition, the γ/γ' phase as an unstable phase is present between the interdendritic regions due to the segregation of alloying elements in the alloy through the solidification stage [32].

3.1.2. Microstructure of weldment

In the fusion zone, the austenitic phase is the prevalent phase after the solidification process. This phase is more stable at room temperature due to the high content of Ni in alloyed materials. As it is known, nickel is one of the strong elements which tends to form the austenitic phase. In the weld metal zone, it can be observed that the microstructure contains dendritic and interdendritic structures. The dendritic cores in the weld-metal region can

be diagnosed through the dark areas illustrated in Figure 6. The solid-liquid zone (Interface) is created during the solidification process. It is difficult to specify this region within a small area between the HAZ and the fusion line due to the mixing of the base alloy with the filler metal, thus creating a region that has a different chemical composition [33]. The granular growth in the HAZ extends towards the fusion boundary in the form of coarse grains, as shown in Figure 7. Near fusion line doesn't indicate the presence of nucleation due to the formation of the epitaxial growth phenomenon, which occurs due to the rapid solidification of the molten welding pool on the solid alloy. In epitaxial solidification mode, partially thawed grains work as pre-existing locations for new grain growth [34]. Coarse columnar grains are diagnosed by SEM inspection and are devoid of liquation cracks, Figure 8a. The solid solution of the gamma phase γ encircles the primary and secondary phases of the γ' phase. Also, it can be observed that MC carbide is located between the interdendritic core, as illustrated in Figure 8b. In the HAZ, certain changes occur in the microstructure due to the thermal influences of the GTAW process. These morphology transformations and irregular distribution of the γ' phase are concentrated in the closer region of the fusion line. These changes in the HAZ rely on the amount of thermal exposure and cooling rate during the welding process [35, 36]. At elevated-temperatures, MC carbide can interact with the matrix phase γ to form new depositions of $M_{23}C_6$ carbides. This decomposition of MC carbide occurs at a temperature of less than 800 °C. Over 850 °C, the MC carbide interacts with the gamma matrix γ to produce $M_{23}C_6$ carbide and the γ' phase [37]. Also, in the root weld-metal zone, there is a lack of penetration of the weld metal, as presented in Figure 9. The high content of Mo in the weld metal region causes embrittlement at the grain boundaries of the welded joints. Thus, the inflow amount of molten material reduces the penetration [38].

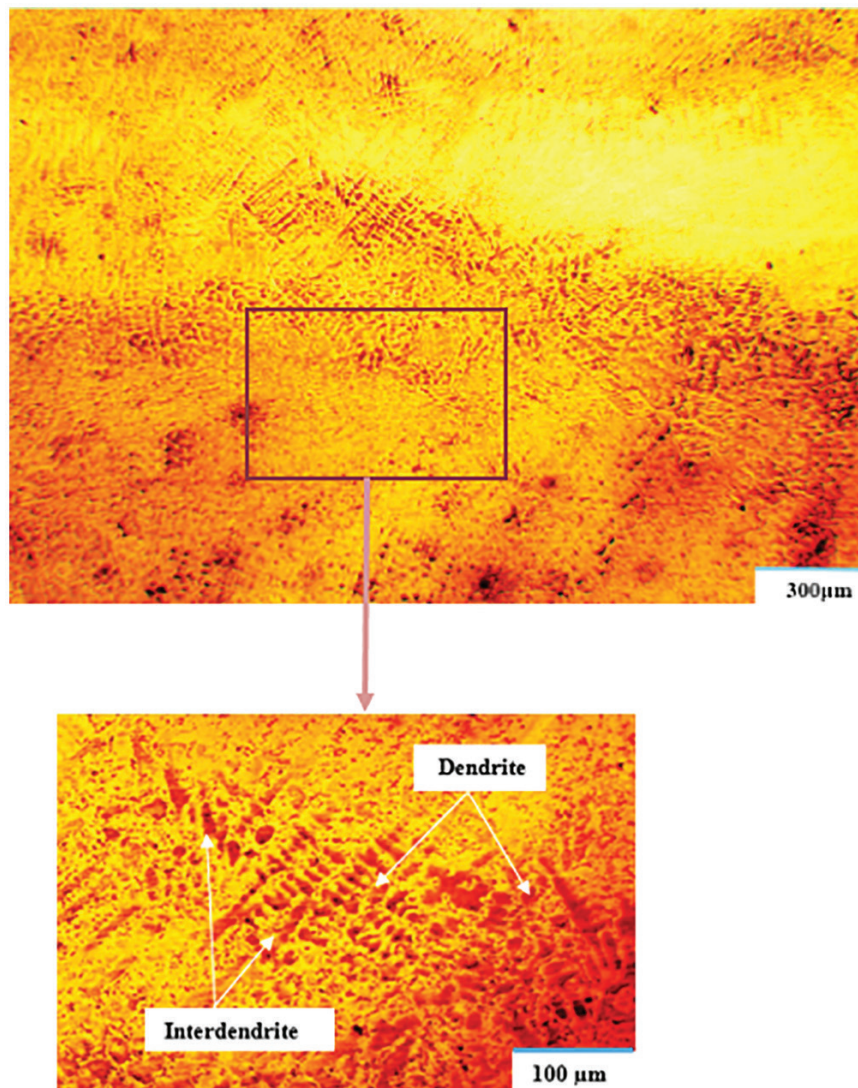


Figure 6: Microstructure image showing dendritic and interdendritic structures at the weld-metal zone using the filler alloy ERNiCrMo-3.

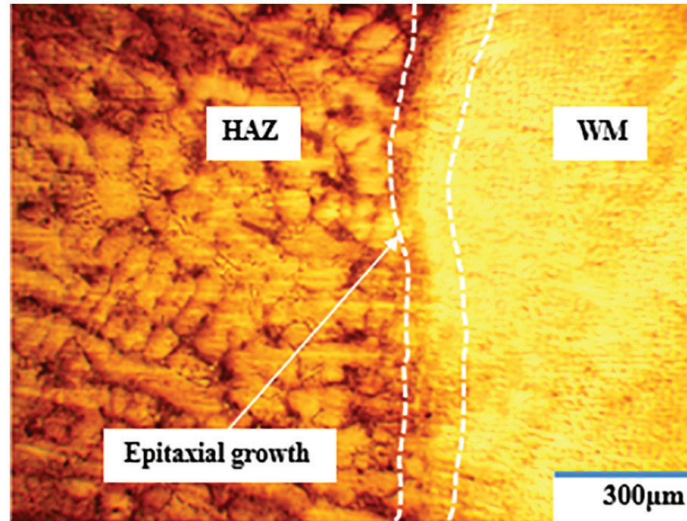


Figure 7: Microstructure image showing the epitaxial solidification of ASTM Mar-M247 weldment.

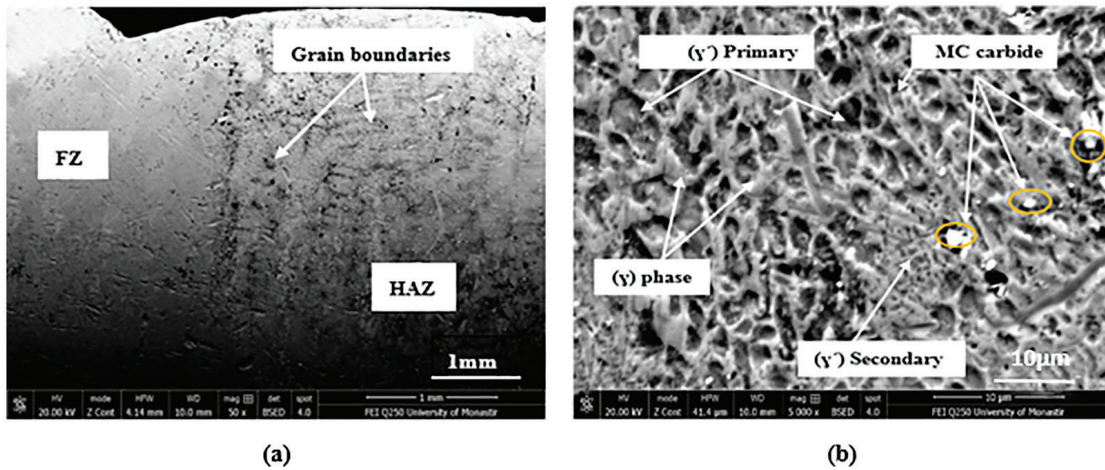


Figure 8: Images microstructure showing the HAZ of ASTM Mar-M247 weldment: (a) columnar grains near the fusion line (b) bimodal distribution of the primary and secondary γ' phase.

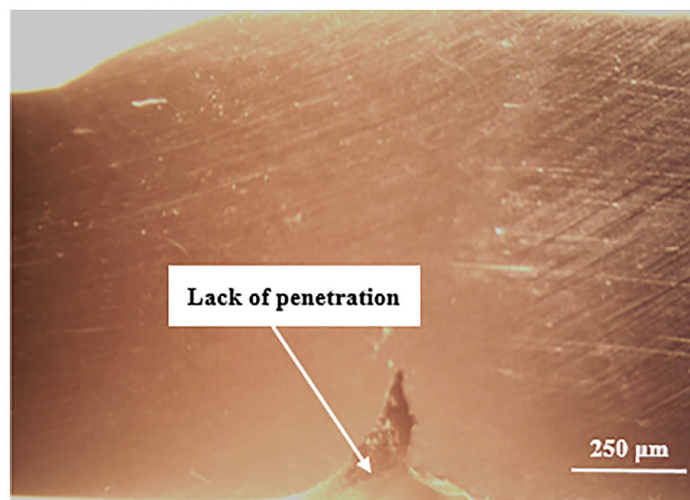


Figure 9: Stereoscope image showing incomplete in the fusion and lack of penetration of the weld–metal in the root weld zone.

3.2. X-ray diffraction inspection results

The X-ray diffraction analysis was applied to ASTM Mar-M247 alloy and also to weld deposits by ERNi-CrMo-3. The X-ray analysis doesn't indicate the presence of the gamma prime γ' in the base alloy as shown in Figure 10. Due to the long service life of this blade, the precipitated particles of the γ' phase lose coherence with the γ matrix, thereby causing damage to the alloy. The topologically close pack (TCP) phase was found by the intermetallic compound Ni_3Cr_2 . This crystalline compound represents a detrimental phase due to its ability to deplete the reinforcing elements in the alloy [25, 26]. In the welded specimen of ASTM Mar-M247 alloy by the filler alloy AWS ERNiCrMo-3, the X-ray diffraction inspection revealed the predominant phases, including NiCr and NiCrCoMo, as solid solutions, as illustrated in Figure 11.

3.3. Line mapping analysis along the welded specimen of Mar-M247 alloy

This test reveals the diffusion of elements along a cross-section of the welded specimen, as shown in Figure 12. In the weld metal region, the homogenous distribution of Ni supports the strong presence of the austenitic phase in the fusion zone. In addition, Cr content gradually increases from the HAZ towards the weld-metal zone and diffuses to 17% in the weld-metal region. Also, the results confirm the prevalence of other alloying

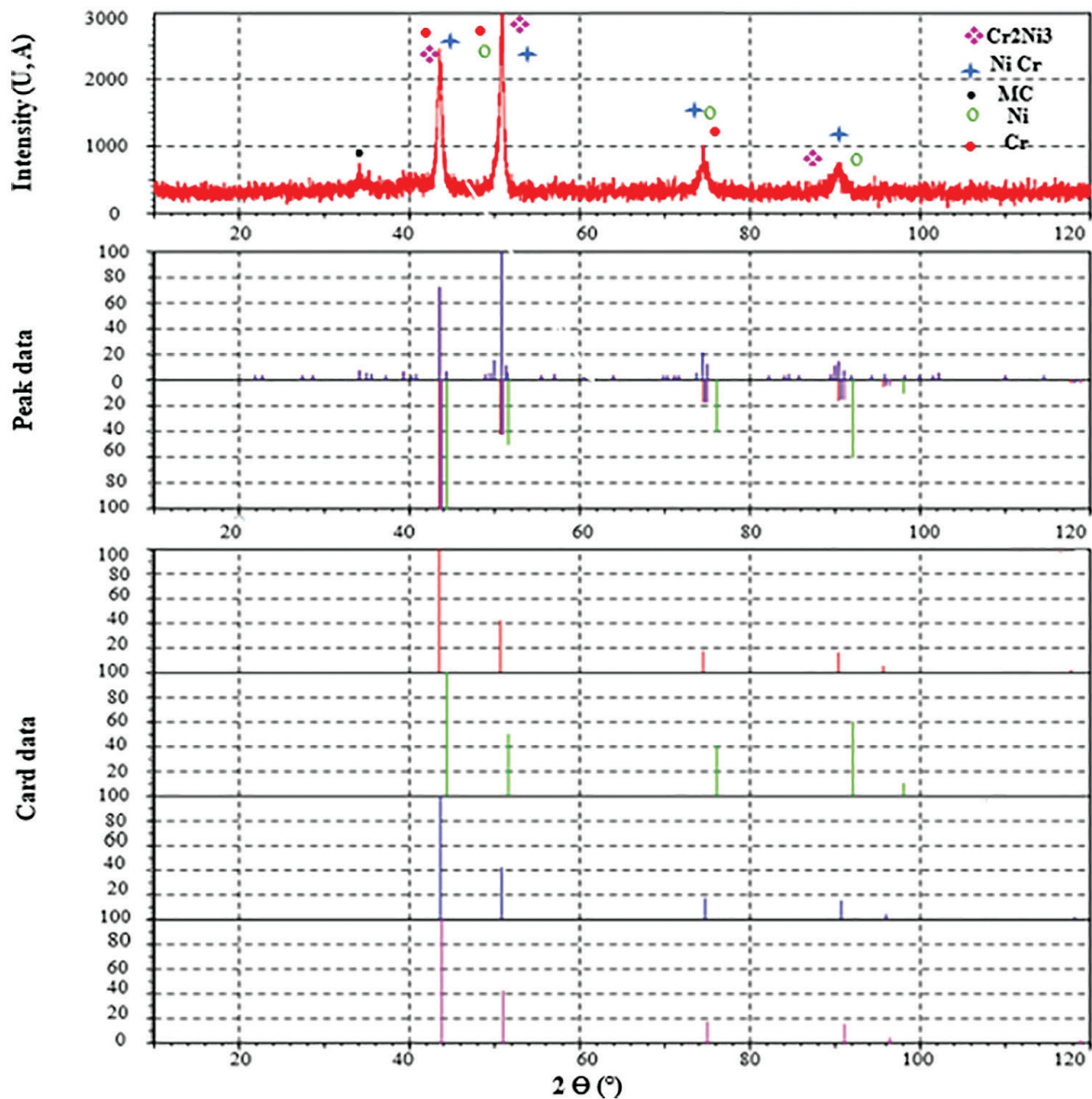


Figure 10: XRD results of the Mar-M 247 alloy.

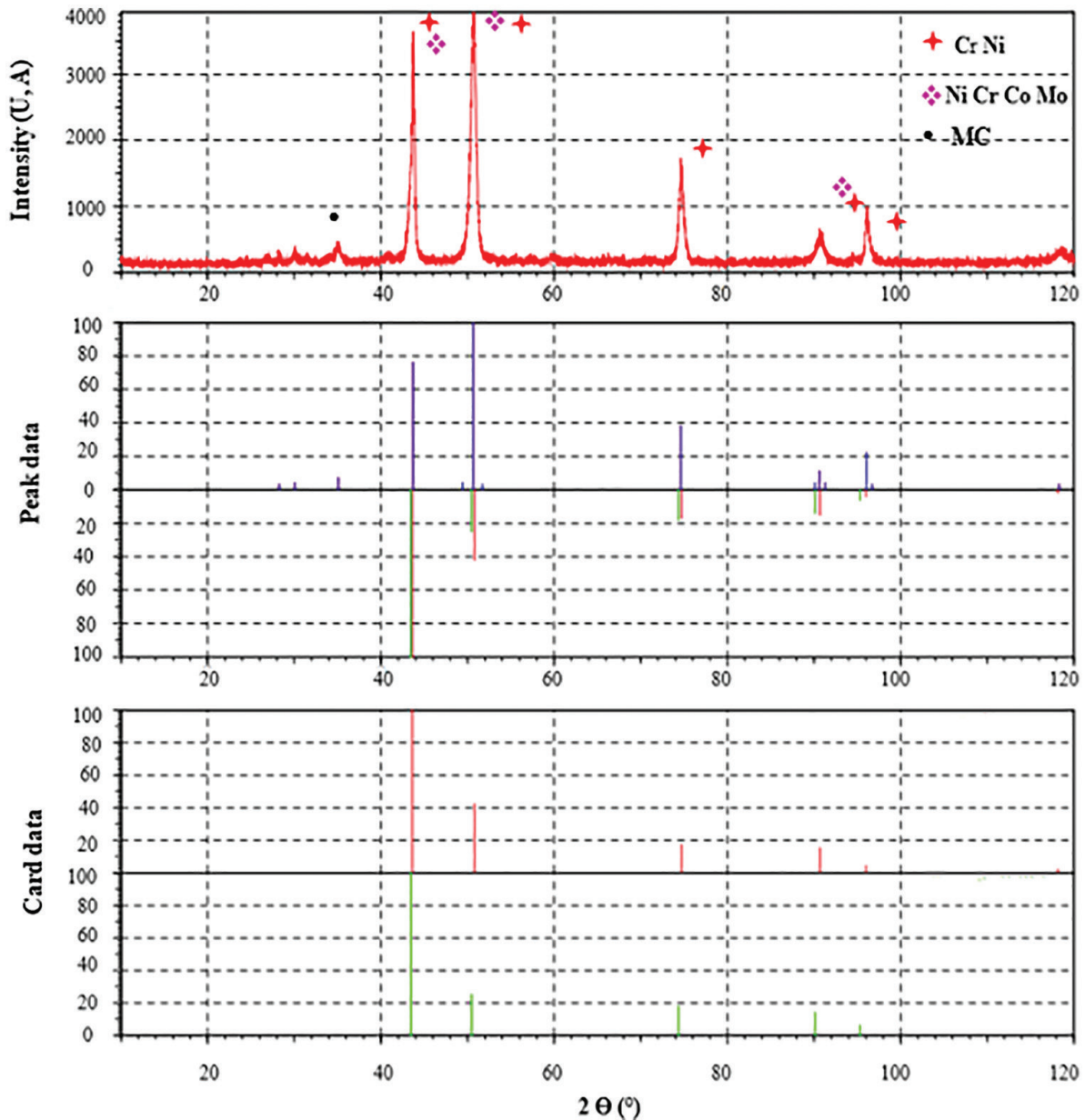


Figure 11: XRD results of ASTM Mar-M 247 weldment by ERNiCrMo-3.

elements like Co, W, Ti, and Al across the weld zones. The content of W diffused towards the melting zone due to the dilution phenomenon. The analysis reveals the gradual decrease in the content of Al and Co from the HAZ towards the melting region due to the segregation of elements during the solidification process. Also, Ni content decreases due to the formation of TCP phases, and carbides precipitate in the HAZ, which leads to the depletion of alloying elements. The diffusion of these elements depends on the coefficient of segregation (K). Ni, Al, Ti, and Nb elements have $K > 1$, which tend to segregate towards the dendritic core. Additionally, it is anticipated that the solid will reject the solute from the liquid during the solidification stage. The solid absorbs the solute when $K > 1$, which tends to segregate towards interdendritic zones [39, 40]. In the root welding region, it can be observed the diffusion of elements Ni, Al, Co, and Ti as detailed in Figure 13. Cr content gradually increases in the root weld-metal, whereas Mo content continuously diffuses along the root weld-metal zone. The solubility of Nb in Ni can be determined by the segregating of Nb at grain boundaries, which is affected by the content of alloying elements. Also, the high Mo content in the weld-metal zone improves creep resistance, thereby reducing the dislocations that occur at high temperatures. [41, 42]. In addition, some elements including C, Nb, and Ti tend to insulate towards the grain boundaries and form strong carbides such as NbC and TiC.

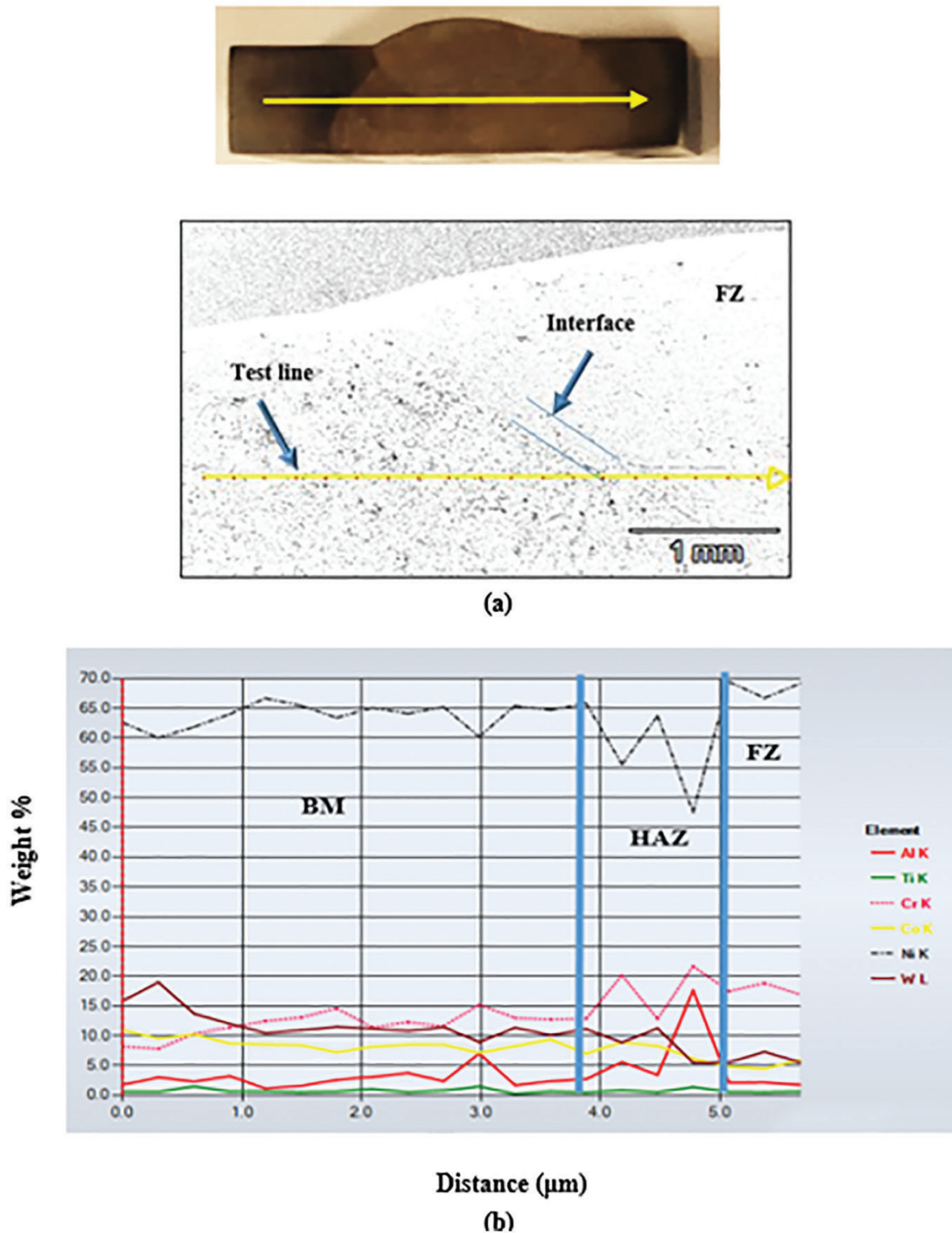
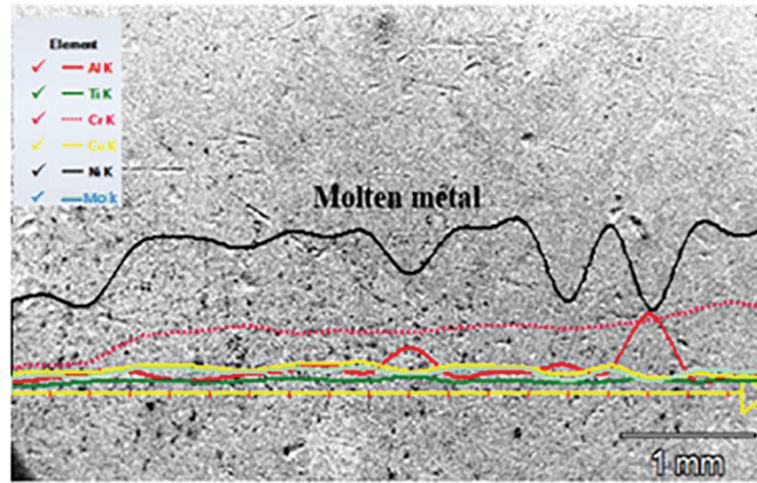


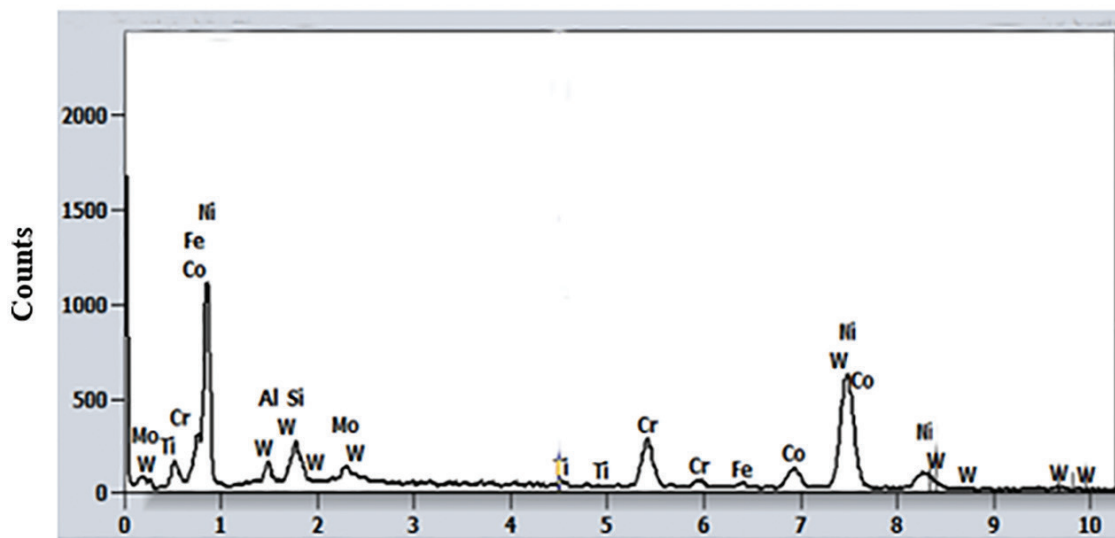
Figure 12: (a) Line analysis (b) line mapping analysis of ASTM Mar-M247 weldment by ERNiCrMo-3.

3.4. Microhardness results

Microhardness analyses were conducted across the center line of the cross-section of the welded specimen, indicating the difference in the average hardness via the base metal, HAZ, and the fusion zone as illustrated in Figure 14. The highest average of hardness was found in the HAZ, which reaches 340HV due to the thermal effects of the weld and the agglomeration of carbides. In contrast, the hardness of the base alloy and the fusion metal is 322HV and 284HV, respectively.



(a)



KeV

(b)

Figure 13: (a) Line mapping analysis (b) EDS diagram at the root weld metal zone of ASTM Mar-M247 weldment by ERNiCrMo-3.

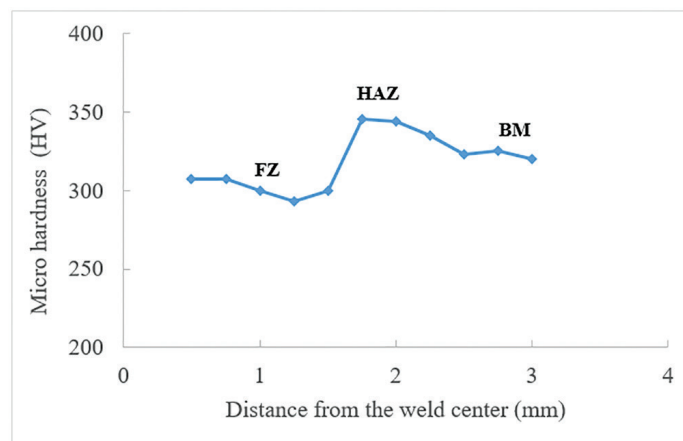


Figure 14: Vickers hardness distribution across the welded joint of ASTM Mar-M247 alloy using ERNiCrMo-3 as a filler alloy.

4. CONCLUSIONS

The cast gas turbine blade of type ASTM Mar-M247 superalloy was welded using ER NiCrMo-3 filler alloy by GTAW. This paper is one of the important topics that aims to study the microstructure of the welded joints of a gas turbine blade. This study consists of the following conclusions:

- Obtaining welded joints of ASTM Mar-M247 superalloy by GTAW which are free of solidification cracks using AWS ErNiCrMo-3 as a filler alloy.
- In the weld-metal region, the austenitic phase is the dominant phase after the solidification process, with dendritic and interdendritic structures in the microstructure. Also, the γ' phase was not observed in the weld metal.
- The content of Al and Co decreases gradually from the HAZ towards the fusion zone, when compared to the base metal due to the segregation during the welding process.
- Coarse precipitated particles of gamma prime γ' phase and irregular distribution are found in the HAZ due to the thermal effects of the GTAW.
- The average microhardness in the HAZ is higher than the base metal and the weld-metal zone, the hardness in HAZ is 340 HV, while it is 322 HV, and 284 HV in the base metal and fusion regions respectively.

5. ACKNOWLEDGMENTS

The authors express their gratitude to Baghdad South Power Station for supplying them with samples of used gas turbine blades.

6. BIBLIOGRAPHY

- [1] BOR, H.Y., WEI, C.N., JENG, R.R., *et al.*, “Elucidating the effects of solution and double ageing treatment on the mechanical properties and toughness of MAR-M247 superalloy at high temperature”, *Materials Chemistry and Physics*, v. 109, n. 2–3, pp. 334–341, 2008. doi: <http://dx.doi.org/10.1016/j.matchemphys.2007.11.041>.
- [2] RAKOCZY, L., GRUDZIEN-RAKOCZY, M., CYGAN, R., *et al.*, “Analysis of the as-cast microstructure and properties of the Ni-based superalloy MAR-M247® produced via directional solidification”, *Metallurgical and Materials Transactions. A, Physical Metallurgy and Materials Science*, v. 54, n. 9, pp. 1–23, 2023. doi: <http://dx.doi.org/10.1007/s11661-023-07123-8>.
- [3] SMID, M., KUNZ, L., HUTAŘ, P., *et al.*, “High cycle fatigue of nickel-based superalloy MAR-M 247 at high temperatures”, *Procedia Engineering*, v. 74, pp. 329–332, Jan. 2014. doi: <http://dx.doi.org/10.1016/j.proeng.2014.06.273>.
- [4] WEE, S., DO, J., KIM, K., *et al.*, “Review on mechanical thermal properties of superalloys and thermal barrier coating used in gas turbines”, *Applied Sciences (Basel, Switzerland)*, v. 10, n. 16, pp. 5476, Aug. 2020. doi: <http://dx.doi.org/10.3390/app10165476>.
- [5] MAZUR, Z., LUNA, A., JUA, J., “Metallurgical assessment of degradation of a gas turbine bucket made of Inconel 738LC alloy after 24000 h in service”, In: *ASME Power Conference*, pp. 325–331, Jan. 2004.
- [6] SUN, Z., JIANG, X., QIU, C., *et al.*, “The investigations of rejuvenation heat treatment on the microstructure and mechanical properties of a serviced gas turbine blade”, *Journal of Alloys and Compounds*, v. 948, pp. 169759, 2023. doi: <http://dx.doi.org/10.1016/j.jallcom.2023.169759>.
- [7] PALLOS, K.J., *Gas turbine repair technology*, Atlanta, GE Power Systems, 2001.
- [8] CHOWDHURY, T.S., MOHSIN, F.T., TONNI, M.M., *et al.*, “A Critical review on gas turbine cooling performance and failure analysis of turbine blades”, *International Journal of Thermofluids*, v. 18, pp. 100329, 2023. doi: <http://dx.doi.org/10.1016/j.ijft.2023.100329>.
- [9] OLLA, A.H., ABBAS, K.H., EMAD, S.A., *et al.*, “Welding procedures of turbine blades by using ER 309L austenitic filler wire”, *Journal of Engineering Technology*, v. 35, n. 1, pp. 68–75, 2017. doi: <http://dx.doi.org/10.30684/etj.2017.127312>.
- [10] HAN, K., WANG, H., PENG, F., *et al.*, “Investigation of microstructure and mechanical performance in IN738LC joint by vacuum electron beam welding”, *Journal of Vacuum*, v. 162, pp. 214–227, Apr. 2019. doi: <http://dx.doi.org/10.1016/j.vacuum.2018.12.047>.
- [11] AL-NAFEAY, R.H., AL-ROUBAIY, A.O., OMIDVAR, H., “Overview of joining and repairing techniques of ni-based superalloy for industrial gas turbine applications”, *Materials Science and Engineering*, v. 1094, n. 1, pp. 012141, 2021.

- [12] ALFRED, I., NICOLAUS, M., HERMSDORF, J., *et al.*, “Advanced high-pressure turbine blade repair technologies”, *Journal of Procedia Cirp*, v. 74, pp. 214–217, 2018. doi: <http://dx.doi.org/10.1016/j.procir.2018.08.097>.
- [13] KVAPIOVA, M., DVORAK, J., KRAL, P., *et al.*, “Creep behavior and life assessment of a cast nickel-base superalloy MAR-M247”, *High-Temperature Materials and Processes*, v. 38, n. 2019, pp. 590–600, 2019. doi: <https://doi.org/10.1515/htmp-2019-0006>.
- [14] POLLNOW, E.N., OSORIO, A.G., ARAUJO, D.B.D., *et al.*, “Microstructural evaluation of a low carbon steel submitted to boriding treatment pre and post GTAW welding”, *Revista Materia*, v. 22, n. 2, pp. e11831, 2017.
- [15] ALVARAES, C.P., MADALENA, F.C.A., SOUZA, L.F.G.D., *et al.*, “Performance of the Inconel 625 alloy weld overlay obtained by FCAW process”, *Revista Matéria*, v. 24, n. 1, pp. e12290, 2019. doi: <http://dx.doi.org/10.1590/s1517-707620190001.0627>.
- [16] SOKKALINGAM, R., PRAVALIKA, B., SIVAPRASAD, K., *et al.*, “Dissimilar welding of high-entropy alloy to Inconel 718 superalloy for structural applications”, *Journal of Materials Research*, v. 37, n. 1, pp. 272–283, Jan. 2022. doi: <http://dx.doi.org/10.1557/s43578-021-00352-w>.
- [17] DOKME, F., KULEKCI, M.K., ESME, U., “Microstructural and mechanical characterization of dissimilar metal welding of inconel 625 and AISI 316L”, *Metals*, v. 8, n. 10, pp. 797, 2018. doi: <http://dx.doi.org/10.3390/met8100797>.
- [18] SAJU, T., VELU, M., “Review on welding and fracture of nickel-based superalloys”, *Materials Today: Proceedings*, v. 46, pp. 7161–7169, 2021. doi: <http://dx.doi.org/10.1016/j.matpr.2020.11.334>.
- [19] CHEN, J.S., LU, Y., LI, X.R., *et al.*, “Gas tungsten arc welding using an arcing wire”, *Welding Journal*, v. 91, n. 10, pp. 261–269, 2012. doi: <http://dx.doi.org/10.3390/ma14237139>.
- [20] KUMAR, A., DIXIT, P.K., “Investigating the effects of filler material and heat treatment on hardness and impact strength of TIG weld”, *Materials Today: Proceedings*, v. 26, pp. 2776–2782, Jan. 2020. doi: <http://dx.doi.org/10.1016/j.matpr.2020.02.578>.
- [21] LI, S., DU, D., ZHANG, L., *et al.*, “A review on filler materials for brazing of carbon-carbon composites”, *Reviews on Advanced Materials Science*, v. 60, n. 1, pp. 92–111, Jan. 2021. doi: <http://dx.doi.org/10.1515/rams-2021-0007>.
- [22] AL-HASSANI, E.S., “Investigation of microstructure and chemical analysis along weldments AISI 410 MSS/ ERNiCrMo-3”, *Journal of Engineering Technology*, v. 36, n. 5, pp. 564–573, 2018. doi: <http://dx.doi.org/10.30684/etj.36.5A.12>.
- [23] XIE, J., MA, Y., OU, M., *et al.*, “Evaluating the microstructures and mechanical properties of dissimilar metal joints between a new cast superalloy K4750 and Hastelloy X alloy by using different filler materials”, *Materials (Basel)*, v. 11, n. 10, pp. 2056, Oct. 2018. doi: <http://dx.doi.org/10.3390/ma11102065>. PubMed PMID: 30360446.
- [24] LEE, H.T., KUO, T.Y., “Analysis of microstructure and mechanical properties in alloy 690 weldments using filler metals I-82 and I-52.”, *Science and Technology of Welding and Joining*, v. 4, n. 2, pp. 94–103, 1999. doi: <http://dx.doi.org/10.1179/136217199101537626>.
- [25] SHARMA, S., TAIWADE, R.V., VASHISHTHA, H., “Investigation on the multi-pass gas tungsten arc welded Bi-metallic combination between nickel-based superalloy and Ti-stabilized austenitic stainless steel”, *Journal of Materials Research*, v. 32, n. 16, pp. 3055–3065, 2017. doi: <http://dx.doi.org/10.1557/jmr.2017.235>.
- [26] KARAHAN, T., MERT, T., TUMER, M., *et al.*, “Microstructural analysis of Inconel 625 nickel alloy/ UNS S31803 duplex stainless-steel dissimilar weldments”, *Advanced Technologies & Materials*, v. 44, n. 1, pp. 15–20, 2019. doi: <http://dx.doi.org/10.24867/ATM-2019-1-003>.
- [27] AMERICAN SOCIETY FOR TESTING AND MATERIALS, *ASTM E407-99: Standard Practice for Microetching Metals and Alloys*, West Conshohocken, ASTM International.
- [28] VANDER VOORT, G., MANILOVA, E., LUCAS, G.M., “Metallographic techniques for superalloys”, *Microscopy and Microanalysis*, v. 10, n. S02, pp. 690–691, Aug. 2004. doi: <http://dx.doi.org/10.1017/S1431927604883442>.
- [29] SZCZOTOK, A., RODAK, K., “Microstructural studies of carbides in MAR-M247 nickel-based superalloy”, *IOP Conference Series. Materials Science and Engineering*, v. 35, n. 1, pp. 012006, 2012. doi: <http://dx.doi.org/10.1088/1757-899X/35/1/012006>.

- [30] SIFI, O., DJEGH, M.E., MEBDOUA, Y., *et al.*, “The effect of the solution and aging treatments on the microstructures and microhardness of nickel-based superalloy”, *Applied Physics (Berlin)*, v. 126, pp. 1–11, May. 2020.
- [31] LU, G.X., LIU, J.D., ZHOU, Y.Z., *et al.*, “Differences in the micromechanical properties of dendrites and interdendritic regions in superalloys”, *Philosophical Magazine Letters*, v. 96, n. 12, pp. 461–468, 2016. doi: <http://dx.doi.org/10.1080/09500839.2016.1252860>.
- [32] RAKOCZY, L., GRUDZIEN, M., ZIELINSKA, L., “Contribution of microstructural constituents on hot cracking of MAR-M247 nickel-based superalloy”, *Archives of Metallurgy and Materials*, v. 63, n. 1, pp. 181–189, 2018. doi: <http://dx.doi.org/10.24425/118926>.
- [33] JOHN, A., JOHNY, K.J., ARULMURUGAN, B., *et al.* “Investigation on microstructure and mechanical properties of corrosion resistance Alloy C-2000 fabricated by conventional arc welding technique”, *SAE Technical Paper*, Oct. 2019. doi: <http://dx.doi.org/10.4271/2019-28-0177>.
- [34] SAADATI, M., NOBARZAD, A.K., JAHAZI, M., “On the hot cracking of HSLA steel welds: role of epitaxial growth and HAZ grain size”, *Journal of Manufacturing Processes*, v. 41, pp. 242–251, May. 2019. doi: <http://dx.doi.org/10.1016/j.jmapro.2019.03.032>.
- [35] Mician, M., Maronek, M., Konar R., *et al.*, “Changes of microstructure and mechanical properties of the HAZ of the S960MC steel sheet weld joint”, *Zavarivanje Nazarene Konstrukcije*, v. 65, n. 3, pp. 113–123, 2020. doi: <http://dx.doi.org/10.5937/zzk2003113M>.
- [36] QIU, C.L., ANDREWS, P., “On the formation of irregular-shaped gamma prime and serrated grain boundaries in a nickel-based superalloy during continuous cooling”, *Materials Characterization*, v. 76, pp. 28–34, Feb. 2013. doi: <http://dx.doi.org/10.1016/j.matchar.2012.11.012>.
- [37] MASHHURIAZAR, A., HAKAN GUR, C., SAJURI, Z., *et al.*, “Effects of heat input on metallurgical behavior in HAZ of multi-pass and multi-layer welded IN-939 superalloy”, *Journal of Materials Research and Technology*, v. 15, pp. 1590–1603, Nov. 2021. doi: <http://dx.doi.org/10.1016/j.jmrt.2021.08.113>.
- [38] SUN, Y.L., OBASI, G., HAMELIN, C.J., *et al.*, “Effects of dilution on alloy content and microstructure in multi-pass steel welds”, *Journal of Materials Processing Technology*, v. 265, pp. 71–86, 2019. doi: <http://dx.doi.org/10.1016/j.jmatprotec.2018.09.037>.
- [39] SZCZOTOK, A., CHMIELA, B., “Effect of heat treatment on chemical segregation in CMSX-4 nickel-base superalloy”, *Journal of Materials Engineering and Performance*, v. 23, n. 8, pp. 2739–2747, 2014. doi: <http://dx.doi.org/10.1007/s11665-013-0843-1>.
- [40] CONSTABLE, D., TER, B., ANDRIEU, E., “Diffusion and segregation of niobium in fcc-nickel”, *Journal of Physics*, v. 24, n. 9, pp. 095010, Feb. 2012. doi: <http://dx.doi.org/10.1088/0953-8984/24/9/095010>. PubMed PMID: 22322788.
- [41] ZHANG, L.L., ZHANG, L.J., LONG, J., *et al.*, “Effects of titanium on grain boundary strength in molybdenum laser weld bead and formation and strengthening mechanisms of brazing layer”, *Materials & Design*, v. 169, pp. 107681, 2019. doi: <http://dx.doi.org/10.1016/j.matdes.2019.107681>.
- [42] ZHANG, J., LI, J., JIN, T., *et al.*, “Effect of Mo concentration on creep properties of a single crystal nickel-base superalloy”, *Materials Science and Engineering A*, v. 527, n. 13–14, pp. 3051–3056, 2010. doi: <http://dx.doi.org/10.1016/j.msea.2010.01.045>.